Geochemical Perspectives Letters

Bridging the depleted MORB mantle and the continental crust using titanium isotopes

Z. Deng, F. Moynier, P.A. Sossi, M. Chaussidon

Supplementary Information

The Supplementary Information includes:

- Materials
- Methods
- Supplementary Text
- Tables S-1 and S-2
- Figures S-1 and S-2
- Supplementary Information References

Materials

The Ti isotopic composition of four geological reference materials from the Geological Survey of the USA, including a Hawaiian basalt (BHVO-2), an Icelandic basalt (BIR-1), a Columbia River basalt (BCR-2) and a Guano Valley andesite (AGV-1) were analysed. Komatiites were collected from five cratons over the world (Pilbara, Kaapvaal, Zimbabwe, Yilgarn and Superior), and have eruption ages of 3.5-2.7 Ga (Table S-1). Only the freshest samples showing spinifex textures and also the chemical compositions closest to the parental magmas were chosen. Details on the samples can be found in Sossi *et al.* (2016). MORB samples from multiple mid-ocean ridges, including five N-MORB and five E-MORB, which have been studied for Cu isotopes in Savage *et al.* (2015) (Table S-1).

Methods

The powders of komatiites (≈ 100 mg) were dissolved following a Parr bomb digestion method described in Sossi *et al*. (2016). Around 11 to 48 mg rock powders of the rock standards and MORB samples were dissolved in 7 ml Savillex PFA beakers with 2 ml 26 M HF and 1 ml 16 M HNO_3 at 120 °C on a hotplate for three days. After drying down, the samples were dissolved in 3 ml 6 M HCl at 130 °C to decompose the fluorides.

The sample aliquots containing 2 to 6 μg Ti were spiked with a prepared ^{47}Ti-^{49}Ti double spike, and were then heated at 100 °C to reach sample-spike homogenisation. Afterwards, the sample solutions were dried down, and the re-dissolved sample solutions were subjected to a three-step ion-exchange chromatographic procedure, including Eichrom DGA (50-100 μm particle size) and Bio-Rad AG1-X8 (200-400 mesh) resins, to remove the matrices from Ti (Deng *et al*., 2018). The Ti isotopic composition of the purified Ti fraction was then measured by a Thermo-Fisher Neptune multi-collector inductively-coupled-plasma mass-spectrometer (MC-ICP-MS) housed at the Institut de Physique du Globe de Paris (France). The sample solutions containing ~300 ppb of natural Ti were introduced in the MC-ICP-MS in 0.5 M HNO_3 + 0.0015 M HF *via* an APEX HF desolvating nebulizer (Elemental Scientific Inc. USA). A spiked IPGP-Ti standard was analysed in between each two analyses of unknown samples for the secondary normalisation. The intensities of $^{44}Ca^+$, $^{46}Ti^+$, $^{47}Ti^+$, $^{48}Ti^+$ and $^{49}Ti^+$ were monitored simultaneously under a medium mass resolution (M/ΔM ≈ 5800) with a static mode. After the correction of Ca isobaric interferences, the signals of $^{46}Ti^+$, $^{47}Ti^+$, $^{48}Ti^+$ and $^{49}Ti^+$ were used for spike inversion in the IsoSpike software developed by Creech and Paul (2015). The derived data are reported with the δ-notation relative to the standards, IPGP-Ti or OL-Ti, and expressed in ‰:

$$d^{49}Ti_{standard} = \left[\frac{\left({}^{49}Ti / {}^{47}Ti \right)_{sample}}{\left({}^{49}Ti / {}^{47}Ti \right)_{standard}} - 1 \right] \times 1000 \qquad \text{Eq. S-1}$$

Supplementary Text

Results and inter-laboratory data comparison

Due to the presence of the small amount of isotopically fractionated Ca within the double spike, a correction of 0.022 ± 0.009 ‰ (2 se, n = 9) on the $\delta^{49}Ti_{IPGP-Ti}$ value has been conducted for all the samples. This change does not affect the isotopic difference between samples in this study. However, if aiming for high-precision inter-laboratory comparison, the analytical uncertainties of ± 0.009 ‰ from the correction of Ca effects and ± 0.011 ‰ from the calibration between IPGP-Ti and OL-Ti have to be propagated onto the corrected or re-normalised values (Deng *et al*., 2018). After all these corrections, the $\delta^{49}Ti$ values of four rock standards (BHVO-2, BIR-1, BCR-2, AGV-1), which without specification would stand for the normalization to OL-Ti standard, are consistent with the reported values in Millet *et al*. (2016) within uncertainty (Table S-1). In addition, the N-MORB samples reported here exhibit an average $\delta^{49}Ti$ value of +0.000 ± 0.008 ‰ (2 se, n = 5) or +0.000 ± 0.016 ‰ if propagating all the uncertainties above, which is in agreement with the N-MORB average value reported in Millet *et al.* (2016), *i.e.* $\delta^{49}Ti$ = +0.002 ± 0.005 ‰ (2 se, n = 7; Table S-2; Fig. S-1). These corroborate the accuracy of the method in this study.

Komatiites are characterised by a progressive depletion in both the light rare earth elements and heavy Ti isotopes with time (Figs. 1 and 2). In detail, the 3.5-3.3 Ga komatiites have $(La/Sm)_N$ values of 0.91-1.02, with subscript 'N' denoting a normalisation to the primitive mantle values from McDonough and Sun (1995), and an average $\delta^{49}Ti$ value of +0.038 ± 0.018 ‰ (2 se, n = 4). The 2.9-2.7 Ga komatiites show the lower $(La/Sm)_N$ values of 0.37-0.78 and a lower average $\delta^{49}Ti$ value of +0.003 ± 0.013 ‰ (2 se, n = 5) (Fig. 1; Table S-1). Although being reported with a larger analytical uncertainty of ± 0.035 ‰ (95 % confidence interval), similar systematics appears between the komatiite samples reported by Greber *et al*. (2017a), *i.e.* the komatiites with the primitive mantle trace element patterns tend to be isotopically heavier than depleted komatiites (Fig. S-1; Table S-2).

The average $\delta^{49}Ti$ values for chondrites in Deng *et al.* (2018) and Williams (2014) are 0.04-0.06 ‰ higher than the chondrite average in Greber *et al.* (2017a). Although the cause of the inter-laboratory discrepancy for chondrites and komatiites is not fully resolved yet (Deng *et al*., 2018), there are differences for the two analytical sessions on komatiites and chondrites in Greber *et al*. (2017a). Their first batch including most of chondrite samples has $\delta^{49}Ti$ values lower by 0.01-0.04 ‰ relative to the second batch (which includes the Allende meteorite) (Fig. S-2; Table S-2). The chondrite and komatiite data in this study, Deng *et al*. (2018) and Williams (2014) are more consistent with the results of the second batch in Greber *et al*. (2017a).

Supplementary Tables

Table S-1 Chemical and Ti isotopic compositions of komatiites and MORBs.

Sample	Location/Type/Lithology	Age (Ga)[a]	MgO (wt. %)[a]	TiO_2 (wt. %)[a]	$^{87}Sr/^{86}Sr$[b]	$(La/Sm)_N$[c]	$\delta^{49}Ti_{IPGP\text{-}Ti}$ (‰)[d]	2 s.e.[e]	2 s.e.[f]	$\delta^{49}Ti$ (‰)[g]	2 s.e.[g]	n[h]
Reference standards												
OL-Ti	Ti standard						-0.140		0.011			8
BHVO-2	basalt		9.70	0.96		1.56	-0.137	0.005	0.010	0.003	0.015	10
AGV-1	andesite		1.53	1.05		4.16	-0.049	0.012	0.015	0.090	0.019	7
BIR-1	basalt		9.70	0.96		0.37	-0.188	0.006	0.011	-0.048	0.016	26
BCR-2	basalt		3.59	2.26		2.41	-0.150	0.009	0.012	-0.011	0.017	11
Komatiites												
179/751	Pilbara Craton, Western Australia	3.515	23.54	0.42		1.02	-0.121	0.015	0.018	0.018	0.021	9
331/783	Kaapvaal Craton, South Africa	3.48	26.27	0.42		0.98	-0.087	0.016	0.018	0.053	0.022	12
331/777a	Kaapvaal Craton, South Africa	3.48	25.10	0.41		1.01	-0.089	0.008	0.012	0.050	0.016	4
176/723	Pilbara Craton, Western Australia	3.28	31.13	0.30		0.91	-0.118	0.007	0.011	0.022	0.016	3
B-R1	Zimbabwe Craton, Zimbabwe	2.8	27.72	0.29		0.75	-0.132	0.011	0.015	0.007	0.018	4
B-R2	Zimbabwe Craton, Zimbabwe	2.8	27.54	0.30		0.78	-0.135	0.013	0.015	0.005	0.019	3
SD5/354.5	Yilgarn Craton, Western Australia	2.7	25.72	0.39		0.56	-0.121	0.006	0.011	0.019	0.015	7
422/94	Superior Craton, Canada	2.7	22.41	0.45		0.42	-0.160	0.013	0.016	-0.020	0.020	6
422/95	Superior Craton, Canada	2.7	22.47	0.41		0.37	-0.138	0.014	0.017	0.001	0.020	8
Mid-ocean ridge basalts (MORBs)												
EW9309 2D-1g	Enriched-type, Mid Atlantic Ridge	≈ 0	7.60	2.04	0.704127	1.85	-0.100	0.029	0.031	0.040	0.033	6
DIVA1 15-5	Enriched-type, Mid Atlantic Ridge	≈ 0	5.93	1.16	0.703214	1.72	-0.113	0.015	0.017	0.027	0.021	7
SWIFT DR06-3-6g	Enriched-type, Southwest Indian Ridge	≈ 0	6.20	1.60	0.702900	1.47	-0.112	0.010	0.013	0.028	0.018	6
DIVA1 13-3	Enriched-type, Mid Atlantic Ridge	≈ 0	7.55	1.46	0.703000	1.70	-0.104	0.026	0.027	0.036	0.029	7
SWIFT DR04-2-3g	Enriched-type, Southwest Indian Ridge	≈ 0	6.23	1.49		1.39	-0.094	0.007	0.012	0.046	0.016	6
PAC2 DR38-1g	Normal-type, Pacific Atlantic Ridge	≈ 0	7.57	1.31	0.702465	0.61	-0.151	0.008	0.012	-0.011	0.017	6
MD57 D2-8	Normal-type, Central Indian Ridge	≈ 0	6.91	1.51		0.59	-0.127	0.015	0.017	0.012	0.021	7
SEARISE1 DR04	Normal-type, East Pacific Rise	≈ 0	5.24	1.59	0.702820	0.70	-0.145	0.011	0.014	-0.005	0.018	6
SEARISE2 DR03	Normal-type, East Pacific Rise	≈ 0	6.15	1.21		0.50	-0.137	0.007	0.011	0.002	0.016	6
RD87 DR18-102	Normal-type, Mid Atlantic Ridge	≈ 0	7.39	1.11	0.702298	0.59	-0.137	0.006	0.011	0.003	0.016	6

[a] The MgO and TiO_2 contents of the komatiites samples are from Sossi *et al*. (2016), and those of the MORB samples are from this study.

[b] The Sr isotopic ratios of the MORB samples are from the PetDB Database (http://www.earthchem.org/petdb).

[c] Subscript "N" represents the normalisation to the primitive mantle values in McDonough and Sun (1995). The $(La/Sm)_N$ values of the komatiites are from Sossi *et al*. (2016), and those of the MORBs are from this study.

[d] A correction for 0.022 ± 0.009 ‰ has been conducted for all the samples to account for the effects from the small amount of the highly isotopically fractionated Ca in the used double spike (Deng *et al*. 2018).

[e] The analytical uncertainty from the original measurement duplicates.
[f] The errors from the correction of Ca effects from double spike have been propagated.
[g] The values have been scaled onto the OL-Ti standard using the $\delta^{49}Ti_{IPGP-Ti}$ value of −0.140 ± 0.011 ‰ with error propagation.
[h] Number of measurement duplicate.

Table S-2 Literature Ti isotopic data of MORBs and mantle peridotites from Millet *et al.* (2016), komatiites (Greber *et al.*, 2017a) and Archean TTGs (Greber *et al.*, 2017b).

Sample	Location/Type/Lithology	Age (Ga)	MgO (wt. %)	TiO_2 (wt. %)	$(La/Sm)_N$	$\delta^{49}Ti_{IPGP-Ti}$ (‰)[d]	2 s.e.[d]	$\delta^{49}Ti$ (‰)	2 s.e.	n	Reference
Mid-ocean ridge basalts (MORBs)											
A127D8-2	Normal-type, North Atlantic	≈ 0	9.43	0.81	0.55[a]	-0.143	0.023	-0.003	0.020	1	Millet *et al.* (2016)
A127D11-1	Normal-type, North Atlantic	≈ 0	8.55	1.17	0.55[a]	-0.134	0.023	0.006	0.020	1	Millet *et al.* (2016)
R94-2	Normal-type, EPR	≈ 0	7.59	1.33	0.55[a]	-0.138	0.030	0.002	0.028	1	Millet *et al.* (2016)
R82-1	Normal-type, EPR	≈ 0	9.17	1.06	0.55[a]	-0.138	0.018	0.002	0.014	1	Millet *et al.* (2016)
Sonne12 42a	Normal-type, Pacific	≈ 0	8.23	1.50	0.55[a]	-0.135	0.024	0.005	0.021	1	Millet *et al.* (2016)
MD57 9-1	Normal-type, Indian	≈ 0	8.88	0.98	0.55[a]	-0.150	0.027	-0.010	0.025	1	Millet *et al.* (2016)
MD57 10-1	Normal-type, Indian	≈ 0	6.84	1.68	0.55[a]	-0.129	0.041	0.011	0.040	1	Millet *et al.* (2016)
Mantle peridotites											
Bch9	Alpine serpentinite	?	36.04	0.09	0.55[a]	-0.128	0.033	0.012	0.031	1	Millet *et al.* (2016)
MM15	Alpine serpentinite	?	36.34	0.06	0.55[a]	-0.143	0.030	-0.003	0.028	1	Millet *et al.* (2016)
LZ14b	Alpine serpentinite	?	38.13	0.07	0.55[a]	-0.110	0.025	0.030	0.023	1	Millet *et al.* (2016)
GP13	Beni Bousera peridotite	?	39.79	0.14	0.55[a]	-0.133	0.025	0.007	0.022	1	Millet *et al.* (2016)
Komatiites											
SCH1.1	Schapenburg	3.55	26.5	0.391	0.95	-0.135	0.032	0.005	0.030	4	Greber *et al.* (2017b)
SCH1.5	Schapenburg	3.55	25.9	0.404	0.98	-0.111	0.032	0.029	0.030	4	Greber *et al.* (2017b)
SCH1.6	Schapenburg	3.55	24.8	0.431	1.00	-0.108	0.032	0.032	0.030	4	Greber *et al.* (2017b)
SCH2.1	Schapenburg	3.55	25.2	0.428	0.94	-0.139	0.032	0.001	0.030	8	Greber *et al.* (2017b)
SCH2.2	Schapenburg	3.55	27.5	0.389	0.94	-0.104	0.032	0.036	0.030	4	Greber *et al.* (2017b)
SCH2.3	Schapenburg	3.55	27.2	0.389	0.94	-0.090	0.032	0.050	0.030	4	Greber *et al.* (2017b)
BV03	Komati	3.48	35.3	0.276	1.06	-0.131	0.032	0.009	0.030	8	Greber *et al.* (2017b)
BV04A	Komati	3.48	29.5	0.364	1.04[b]	-0.141	0.032	-0.001	0.030	4	Greber *et al.* (2017b)
BV04B	Komati	3.48	31.3	0.346	1.04[b]	-0.132	0.032	0.008	0.030	4	Greber *et al.* (2017b)
BV05	Komati	3.48	28.2	0.378	1.08	-0.118	0.032	0.022	0.030	4	Greber *et al.* (2017b)
BV06	Komati	3.48	25.3	0.434	0.99	-0.169	0.032	-0.029	0.030	4	Greber *et al.* (2017b)
564-6	Weltevreden	3.26	31.0	0.184	0.62	-0.155	0.036	-0.015	0.034	4	Greber *et al.* (2017b)
501-1b	Weltevreden	3.26	42.7	0.089	0.72	-0.136	0.035	0.004	0.033	4	Greber *et al.* (2017b)

501-2	Weltevreden	3.26	42.8	0.090	0.67	-0.162	0.032	-0.022	0.030	4	Greber *et al.* (2017b)
501-3	Weltevreden	3.26	31.0	0.177	0.67	-0.179	0.032	-0.039	0.030	4	Greber *et al.* (2017b)
501-4	Weltevreden	3.26	34.0	0.161	0.67	-0.157	0.032	-0.017	0.030	4	Greber *et al.* (2017b)
501-8b	Weltevreden	3.26	42.4	0.096	0.67	-0.141	0.035	-0.001	0.033	4	Greber *et al.* (2017b)
TN01	Belingwe	2.7	24.0	0.366	0.75[c]	-0.110	0.036	0.030	0.034	4	Greber *et al.* (2017b)
TN03	Belingwe	2.7	20.3	0.419	0.75[c]	-0.131	0.036	0.009	0.034	4	Greber *et al.* (2017b)
TN21	Belingwe	2.7	29.6	0.283	0.75[c]	-0.123	0.036	0.017	0.034	4	Greber *et al.* (2017b)
ZV10	Belingwe	2.7	27.5	0.308	0.75[c]	-0.135	0.036	0.005	0.034	4	Greber *et al.* (2017b)
ZV14	Belingwe	2.7	16.5	0.463	0.75[c]	-0.123	0.036	0.017	0.034	4	Greber *et al.* (2017b)
M657	Alexo	2.7	19.9	0.50	0.59	-0.174	0.032	-0.034	0.030	4	Greber *et al.* (2017b)
M657b	Alexo	2.7	19.9	0.50	0.59	-0.151	0.035	-0.011	0.033	4	Greber *et al.* (2017b)
M663	Alexo	2.7	28.40	0.34	0.47	-0.214	0.032	-0.074	0.030	4	Greber *et al.* (2017b)
M663b	Alexo	2.7	28.40	0.34	0.47	-0.170	0.035	-0.030	0.033	4	Greber *et al.* (2017b)
M666	Alexo	2.7	27.90	0.35	0.52	-0.200	0.032	-0.060	0.030	4	Greber *et al.* (2017b)
M666b	Alexo	2.7	27.90	0.35	0.52	-0.180	0.035	-0.040	0.033	4	Greber *et al.* (2017b)
M712	Alexo	2.7	39.60	0.21	0.60	-0.175	0.032	-0.035	0.030	4	Greber *et al.* (2017b)
M712b	Alexo	2.7	39.60	0.21	0.60	-0.140	0.035	0.000	0.033	4	Greber *et al.* (2017b)
Tonalite-trondhjemite-granodiorite (TTGs)											
96/201	Kaapvaal Craton, Murchison Belt, South Africa	2.98	0.32	0.28	6.49	0.393	0.032	0.533	0.030		Greber *et al.* (2017a)
96/202	Kaapvaal Craton, Murchison Belt, South Africa	2.98	0.40	0.21	6.06	0.430	0.032	0.570	0.030		Greber *et al.* (2017a)
96/233	Kaapvaal Craton, Murchison Belt, South Africa	2.98	0.23	0.09	7.88	0.369	0.032	0.509	0.030		Greber *et al.* (2017a)
96/246	Kaapvaal Craton, Murchison Belt, South Africa	2.98	0.70	0.31	4.94	0.204	0.032	0.344	0.030		Greber *et al.* (2017a)
96/211	Kaapvaal Craton, Rhenosterkoppies, South Africa	2.98	0.47	0.15	4.36	0.276	0.032	0.416	0.030		Greber *et al.* (2017a)
96/203	Limpopo Southern Marginal Zone, South Africa	2.98	1.64	0.29	6.32	0.126	0.032	0.266	0.030		Greber *et al.* (2017a)
96/225	Limpopo Southern Marginal Zone, South Africa	2.98	1.16	0.46	5.67	0.077	0.032	0.217	0.030		Greber *et al.* (2017a)
96/227	Limpopo Southern Marginal Zone, South Africa	2.98	1.58	0.39	3.53	0.125	0.032	0.265	0.030		Greber *et al.* (2017a)
96/217	Limpopo Southern Marginal Zone, South Africa	2.98	1.10	0.36	5.54	0.174	0.032	0.314	0.030		Greber *et al.* (2017a)
96/230	Limpopo Southern Marginal Zone, South Africa	2.98	4.69	0.60	7.25	0.033	0.032	0.173	0.030		Greber *et al.* (2017a)

[a] The MORB samples in Millet *et al.* (2016) are the normal-type, and the typical average $(La/Sm)_N$ value of 0.55 for N-MORBs is used here. The same value has been assumed for the depleted mantle peridotite samples from Millet *et al.* (2016).

[b] The average average $(La/Sm)_N$ value of the other komatiites from Komatii is shown here.

[c] The typical $(La/Sm)_N$ value of the komatiites from Belingwe in Sossi *et al.* (2016) is shown here.

[d] The values have been scaled onto the IPGP-Ti standard using the $\delta^{49}Ti_{IPGP-Ti}$ value of −0.140 ± 0.011 ‰ with error propagation.

Supplementary Figures

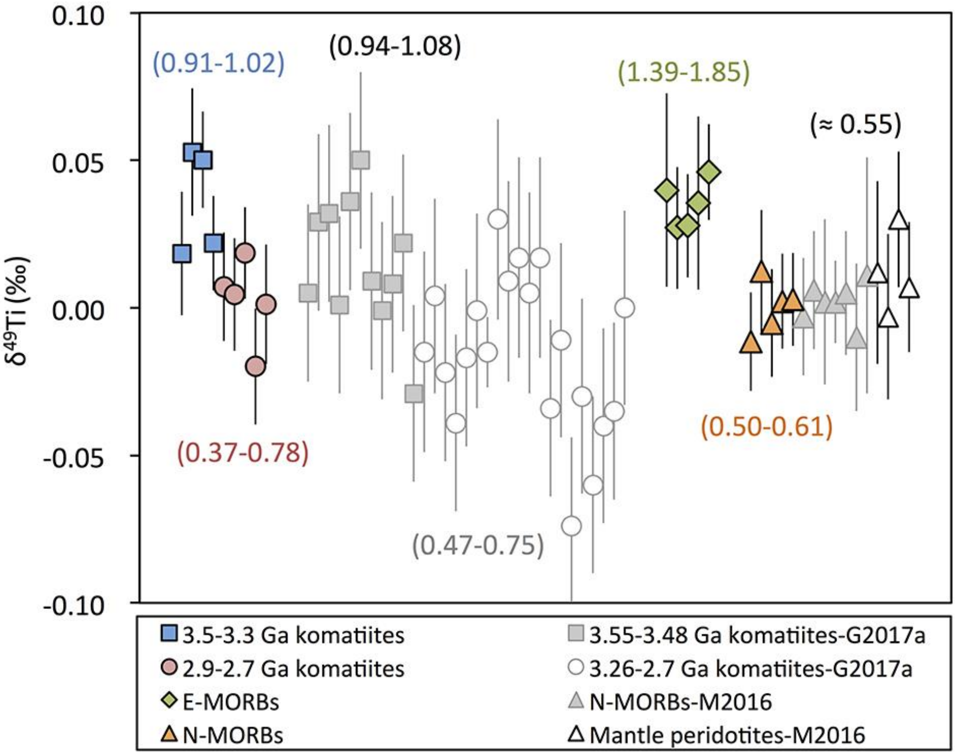

Figure S-1 Comparing the komatiite, MORB and mantle peridotite data of this study with those from Millet *et al*. (2016) and Greber *et al.* (2017a). The $(La/Sm)_N$ range of each group of samples is shown.

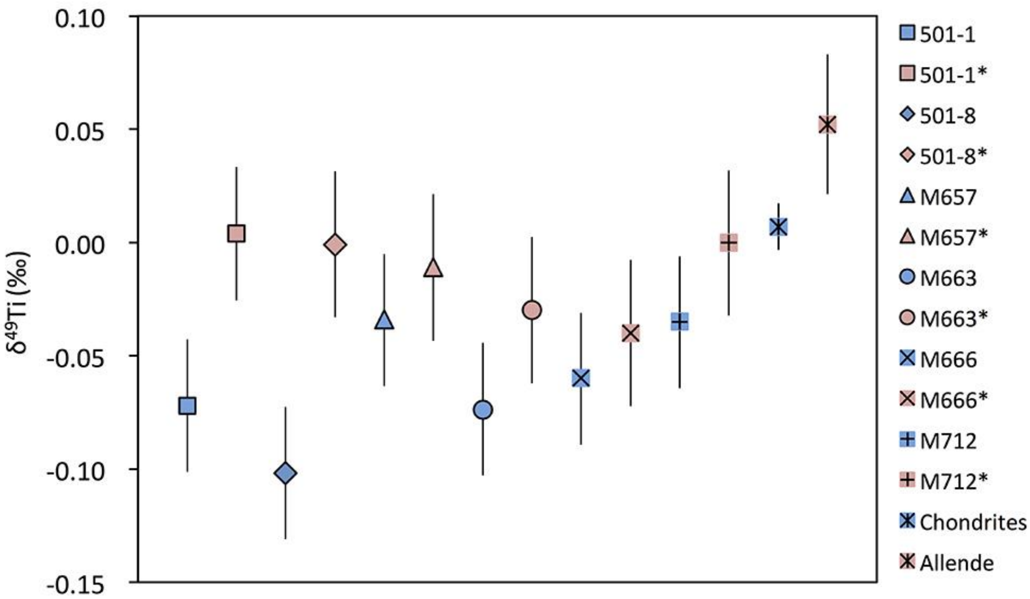

Figure S-2 Comparing the δ^{49}Ti values from two analytical sessions on chondrites and komatiites in Greber *et al*. (2017a). The first batch of dissolutions (blue labels, including most chondrites) provides the lower δ^{49}Ti values than the second batch (pink labels, including Allende meteorite).

Supplementary Information References

Creech, J.B., Paul, B. (2015) IsoSpike: Improved Double-Spike Inversion Software. *Geostandards and Geoanalytical Research* 39, 7–15.

Deng, Z., Moynier, F., van Zuilen, K., Sossi, P.A., Pringle, E.A., Chaussidon, M. (2018) Lack of resolvable titanium stable isotopic variations in bulk chondrites. *Geochimica et Cosmochimica Acta* 239, 409–419.

Greber, N.D., Dauphas, N., Puchtel, I.S., Hofmann, B.A., Arndt, N.T. (2017a) Titanium stable isotopic variations in chondrites, achondrites and lunar rocks. *Geochimica et Cosmochimica Acta* 213, 534–552.

Greber, N.D., Dauphas, N., Bekker, A., Ptáček, M.P., Bindeman, I.N., Hofmann, A. (2017b) Titanium isotopic evidence for felsic crust and plate tectonics 3.5 billion years ago. *Science* 357, 1271–1274.

McDonough, W.F., Sun, S.S. (1995) The composition of the Earth. *Chemical Geology* 120, 223–253.

Millet, M.A., Dauphas, N., Greber, N.D., Burton, K.W., Dale, C.W., Debret, B., Macpherson, C.G., Nowell, G.M., Williams, H.M. (2016) Titanium stable isotope investigation of magmatic processes on the Earth and Moon. *Earth and Planetary Science Letters* 449, 197–205.

Savage, P.S., Moynier, F., Chen, H., Shofner, G., Siebert, J., Badro, J., Puchtel, I.S. (2015) Copper isotope evidence for large-scale sulphide fractionation during Earth's differentiation. *Geochemical Perspectives Letters* 1, 53–64.

Sossi, P.A., Eggins, S.M., Nesbitt, R.W., Nebel, O., Hergt, J.M., Campbell, I.H., O'Neill, H.S.C., Van Kranendonk, M., Davies, D.R. (2016) Petrogenesis and geochemistry of Archean komatiites. *Journal of Petrology* 57, 147–184.

Williams, N.H. (2014) Titanium isotope cosmochemistry. Ph.D. thesis, Manchester University, http://www. escholar.manchester.ac.uk/uk-ac-man-scw:259269.